Role of AMOC in Transient Climate Response to Greenhouse Gas Forcing in Two Coupled Models

AIXUE HU

National Center for Atmospheric Research, Boulder, Colorado

LUKE VAN ROEKEL AND WILBERT WEIJER

Los Alamos National Laboratory, Los Alamos, New Mexico

OLUWAYEMI A. GARUBA

Pacific Northwest National Laboratory, Richland, Washington

WEI CHENG

Joint Institute for the Study of the Atmosphere and Ocean, University of Washington, and NOAA/Pacific Marine Environmental Laboratory, Seattle, Washington

BALU T. NADIGA

Los Alamos National Laboratory, Los Alamos, New Mexico

(Manuscript received 31 December 2019, in final form 7 April 2020)

ABSTRACT

As the greenhouse gas concentrations increase, a warmer climate is expected. However, numerous internal climate processes can modulate the primary radiative warming response of the climate system to rising greenhouse gas forcing. Here the particular internal climate process that we focus on is the Atlantic meridional overturning circulation (AMOC), an important global-scale feature of ocean circulation that serves to transport heat and other scalars, and we address the question of how the mean strength of AMOC can modulate the transient climate response. While the Community Earth System Model version 2 (CESM2) and the Energy Exascale Earth System Model version 1 (E3SM1) have very similar equilibrium/effective climate sensitivity, our analysis suggests that a weaker AMOC contributes in part to the higher transient climate response to a rising greenhouse gas forcing seen in E3SM1 by permitting a faster warming of the upper ocean and a concomitant slower warming of the subsurface ocean. Likewise the stronger AMOC in CESM2 by permitting a slower warming of the upper ocean leads in part to a smaller transient climate response. Thus, while the mean strength of AMOC does not affect the equilibrium/effective climate sensitivity, it is likely to play an important role in determining the transient climate response on the centennial time scale.

1. Introduction

The Atlantic meridional overturning circulation (AMOC) is a global-scale ocean circulation that plays a significant role in modulating the global and regional climate via changes in the redistribution of oceanic heat, salt, and biogeochemical tracers. Studies based on both idealized models and coupled general circulation models suggest that the AMOC may have multiple equilibrium states and changes from one equilibrium state to another may be abrupt, and thus capable of inducing abrupt climate changes around the North Atlantic region and the globe [e.g., Rahmstorf 1996; Stocker and Wright 1991a,b; Stocker et al. 1992; Stouffer et al. 2006; Hu et al. 2010, 2012; for more details see Weijer et al. (2019) and the references therein]. Because of

Supplemental information related to this paper is available at the Journals Online website: https://doi.org/10.1175/JCLI-D-19-1027.s1.

Corresponding author: Aixue Hu, ahu@ucar.edu

DOI: 10.1175/JCLI-D-19-1027.1

the potential abrupt transition of the AMOC from one state to another, it has been a central focus of many studies on both past and future climate changes (e.g., Hu et al. 2004, 2008, 2010, 2012, 2015; Gregory et al. 2005; Stouffer et al. 2006). Given the current upward trend of atmospheric greenhouse gas concentrations, coupled climate models participating in phase 5 of the Coupled Model Intercomparison Project (CMIP5) have projected a decline of AMOC in the twenty-first century and beyond, and the rate of the AMOC's decline depends on the different climate forcing pathways (e.g., Cheng et al. 2013). Most CMIP6 models also projected a significant weakening of the AMOC (Weijer et al. 2020). Here we focus on the role of the AMOC in the transient response of the climate system to changes in greenhouse gas forcing, a topic that has not been fully addressed, using two CMIP6 models: the Community Earth System Model version 2 (CESM2; Danabasoglu et al. 2019) and the Energy Exascale Earth System Model version 1 (E3SM1; Golaz et al. 2019).

Although all CMIP models show a rising of the global mean surface air temperature as greenhouse gas concentration increases, the rate of this warming and the total warming are different from one model to another, which significantly inhibits our ability to accurately assess the potential future climate changes due to changes in greenhouse gas forcing. As indicated by Weijer et al. (2020) and Lin et al. (2019), the equilibrium climate sensitivity (ECS) may be related to the mean AMOC strength (e.g., a lower ECS corresponds to a stronger AMOC). This suggests that the AMOC may play a role in determining the climate response to increased atmospheric CO_2 concentration. Here our interest in CESM2 and E3SM1 is partially motivated by the nearly identical ECS in these two models (Gettelman et al. 2019; Golaz et al. 2019) but the simulated AMOC strength is quite different in their preindustrial control simulations. This result is striking and runs counter to the results of Weijer et al. (2020), and here we suggest that in these two models AMOC could critically impact the transient climate response to rising greenhouse gases and may not as critically impact the ECS.

The rest of the paper is organized as the following: section 2 introduces the models and numerical experiments analyzed in this study; section 3 illustrates the major results; and section 4 is the conclusion.

2. Model and experiments

CESM2 is the newest version of the global climate model developed at National Center for Atmospheric Research in collaboration with scientists from universities and U.S. Department of Energy laboratories (Danabasoglu et al. 2019). Its atmospheric component is the Community Atmospheric Model version 6 (CAM6), the ocean component is the Parallel Ocean Program version 2 (POP2), the sea ice component is the CICE version 5 (CICE5), and the land surface component is the Community Land Model version 5 (CLM5). The horizontal resolution for all components is a nominal 1° and the simulated climate agrees with observations reasonably well [for more model evaluations, please see the CESM2 collection of the *Journal of Advances in Modeling Earth Systems*; https://agupubs.onlinelibrary.wiley.com/doi/toc/10.1002/(ISSN)1942-2466.CESM2].

E3SM1 is a coupled climate model newly developed at U.S. Department of Energy, which was branched from CESM1 (Hurrell et al. 2013) with new component models and improvements in model physics. Its atmospheric model is the E3SM atmospheric model (EAM), which uses a spectral element dynamic core, increased vertical resolution, and significantly modulated model physics in comparison to CAM5; the ocean and sea ice components use the Model for Prediction Across Scales (MPAS) framework; and the land model is a revised version of CLM4.5 with many improvements (Golaz et al. 2019). The horizontal resolution for E3SM1 is also a nominal 1°. The simulated climate also agrees with observations [e.g., Golaz et al. 2019; Petersen et al. 2019; for a collection of E3SM1 publications, please see https://agupubs.onlinelibrary.wiley.com/doi/toc/10.1002/(ISSN)2169-8996.ENERGY1].

Here we primarily analyze the preindustrial control runs, the twentieth-century historical runs (1850–2014), and the idealized 1% CO_2 runs, which are part of the DECK experiments (Diagnostic, Evaluation and Characterization of Klima; Eyring et al. 2016). For the preindustrial control runs, all external forcing is fixed at 1850 level. For twentieth-century runs, time-evolving forcing from all known sources (e.g., solar and volcanic, CO_2, CH_4, SO_x) is used from 1850 to 2014. The 1% CO_2 run is an idealized 150-yr-long simulation with CO_2 concentration increasing 1% per year compound so the CO_2 concentration doubles around model year 70 and quadruples around model year 140. For CMIP6, CESM2 provides a 1200-yr-long preindustrial control run, 11-member ensemble twentieth-century runs, and one 1% CO_2 run; E3SM1 provides a 500-yr preindustrial control run, 5-member ensemble twentieth-century runs, and one 1% CO_2 run. We also include the Shared Socio-Economic Pathways (SSPs) simulations, which CESM2 has published but E3SM1 has not. The SSPs discussed here are SSP1–2.6, SSP2–4.5, SSP3–7.0, and SSP5–8.5. The second number indicates the greenhouse gas–induced radiative forcing by the end of the twenty-first century (in $W\,m^{-2}$).

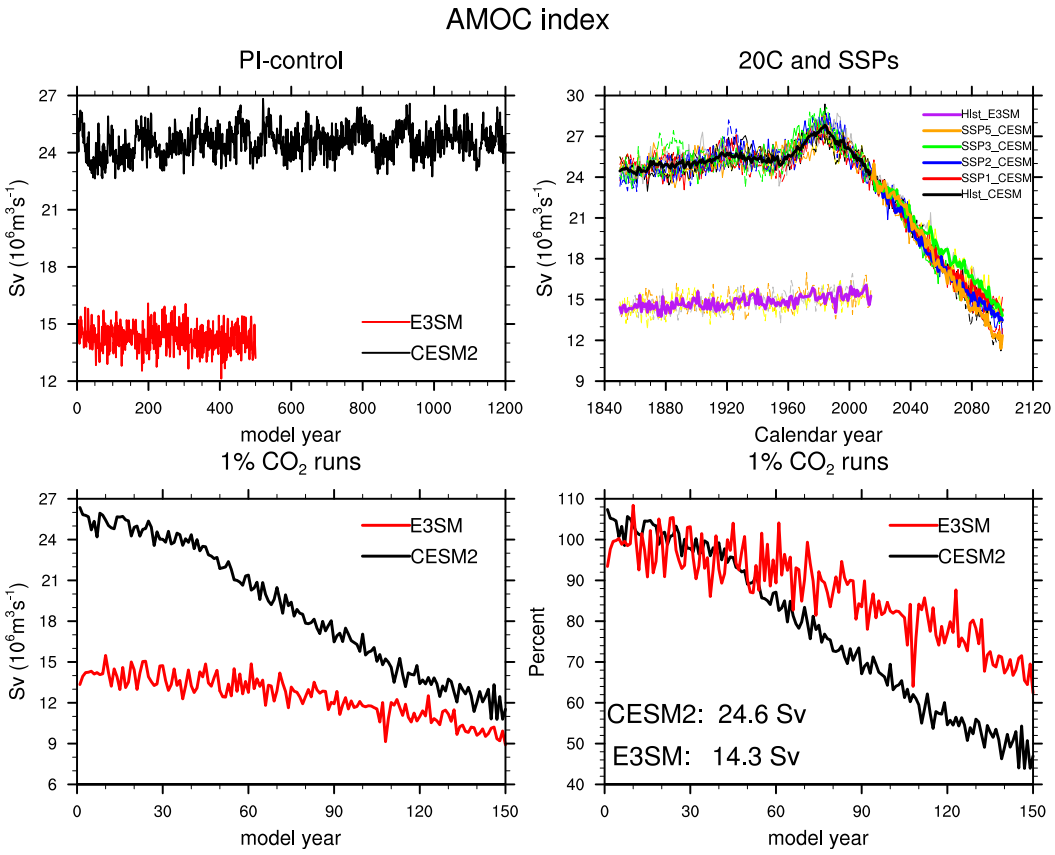

FIG. 1. Time evolution of the AMOC index in the (top left) preindustrial control run, (top right) twentieth-century and future SSP runs, (bottom left) 1% CO_2 runs, and (bottom right) the percentage changes relative to the control run mean in 1% CO_2 runs.

3. Results

a. AMOC mean state and transient changes

Figure 1 shows the time evolution of AMOC in the preindustrial control run, twentieth-century run, and future projection runs (SSPs). The mean strength of the AMOC (defined as the maximum of the Atlantic overturning streamfunction below 500-m depth) in the preindustrial control run is 24.6 Sv (18 Sv at 26.5°N) for CESM2 and 14.3 Sv (9 Sv at 26.5°N) for E3SM1 (1 Sv ≡ $10^6\,m^3\,s^{-1}$). In comparison to the observed estimates (e.g., ~18 Sv at 26.5°N from RAPID-MOCHA based on a 14-yr record, Smeed et al. 2019; Cunningham et al. 2007, 2013; Cunningham and Marsh 2010; Johns et al. 2011), AMOC in CESM2 is very close to the observed value as suggested by the RAPID-MOCHA project and might be slightly on the high side and the AMOC in E3SM1 is surely on the low side and is too weak in comparison to recent observations and simulations from other CMIP6 models (Weijer et al. 2020). In comparison to the CMIP5 models (Collins et al. 2013), the mean AMOC strength in the control run is in the medium to high range for CESM2 and in the low range for E3SM1.

During the historical period (1850–2014), AMOC has a slightly upward trend in both CESM2 and E3SM1 ensembles, and this trend is more obvious in CESM2 than in E3SM1 (Fig. 1 top-right panel; the thick lines are the ensemble mean and thin lines are the individual members). After the mid-1980s, AMOC starts to decline in CESM2 and the rate of AMOC decline is not too different from different future SSPs. Overall, the decline of AMOC is the greatest in SSP5, a scenario with the highest greenhouse gas forcing than the other SSPs.

To better assess the different changes of AMOC under greenhouse gas forcing, here we focus on the comparison of the AMOC in the idealized 1% CO_2 simulations from these two models. AMOC weakens from ~26 Sv at the beginning of the 1% CO_2 run to ~12 Sv at the time of CO_2, quadrupling in CESM2, and from ~14 to ~10 Sv in E3SM1 (Fig. 1 bottom-left panel). Percentagewise, AMOC weakens slightly more than 50% for CESM2, but only roughly 35% for E3SM1 (Fig. 1, bottom-right panel). Therefore, the AMOC

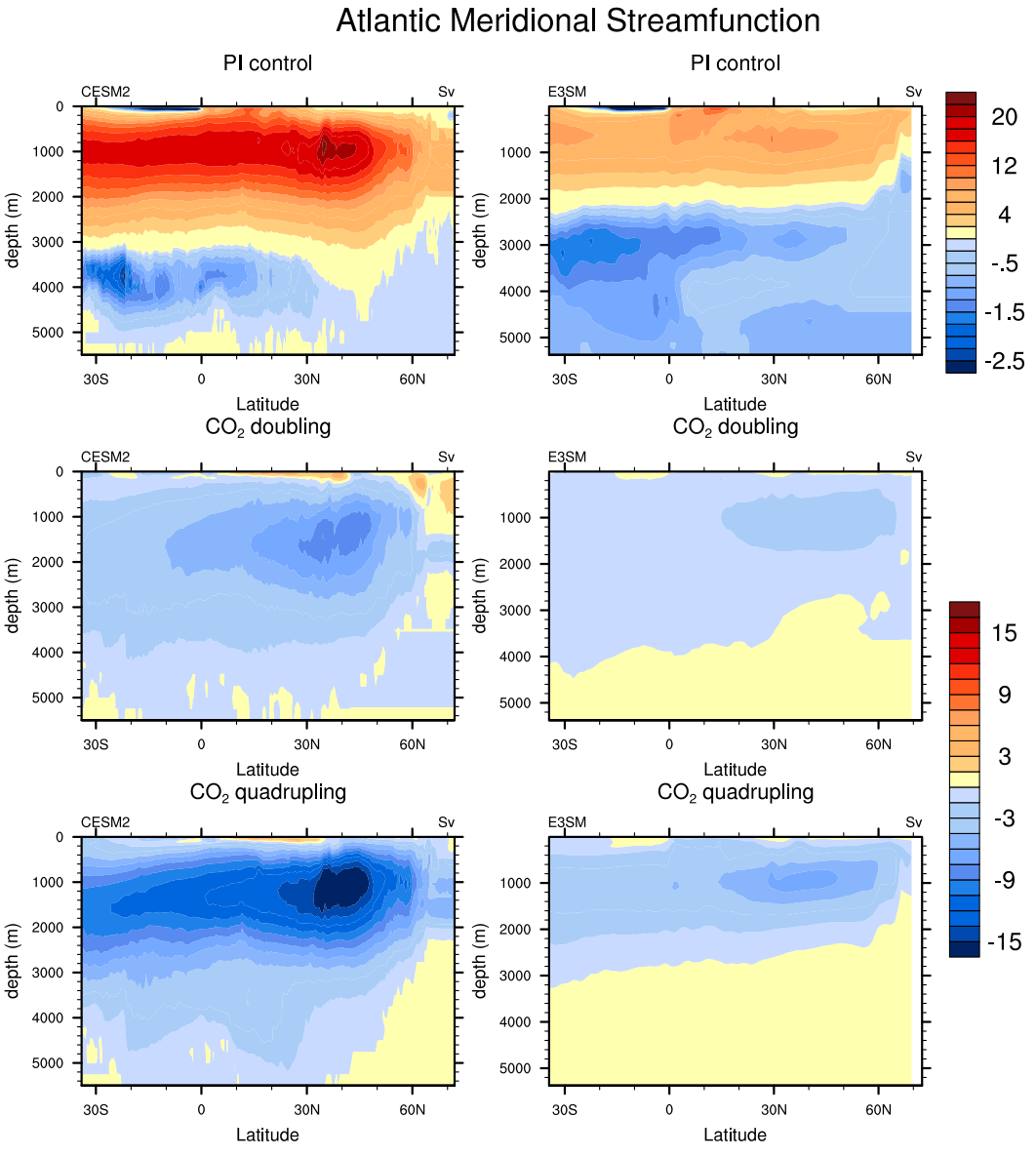

FIG. 2. (top) The Atlantic meridional streamfunction in the control run and the anomaly relative to control run in the 1% CO_2 runs at times of CO_2 (middle) doubling and (bottom) quadrupling. The contour interval for the top row is 2 Sv for the positive values and 0.5 Sv for the negative values; for the middle and bottom rows, the contour interval is 1.5 Sv.

weakens more both in absolute and relative value in CESM2 than in E3SM1. This can be seen more clearly in Fig. 2, which shows the mean Atlantic meridional streamfunction in the control runs and the change of these streamfunctions at times of CO_2 doubling and quadrupling. In CESM2, AMOC in the control run penetrates much deeper than that in E3SM1 (the upper positive cell in the top panels of Fig. 2), such that AMOC reaches a depth of about 3200 m in most parts of the Atlantic basin with a maximum depth over 4000 m around 45°N in CESM2, but only about 2300 m in E3SM1. As indicated by Broecker (1998) and Barker et al. (2009), there is a seesaw-like change between the North and South Atlantic Ocean circulation, such that with a stronger AMOC (upper cell in the top panels of Fig. 2), the Antarctic Bottom Water (AABW) formation in the Southern Ocean (related to the bottom negative cell in the top panels of Fig. 2) would be weaker, and vice versa. The overturning in the top panels of Fig. 2 agree with these previous studies, showing a stronger upper overturning cell (AMOC, related to the North Atlantic Deep Water formation, or

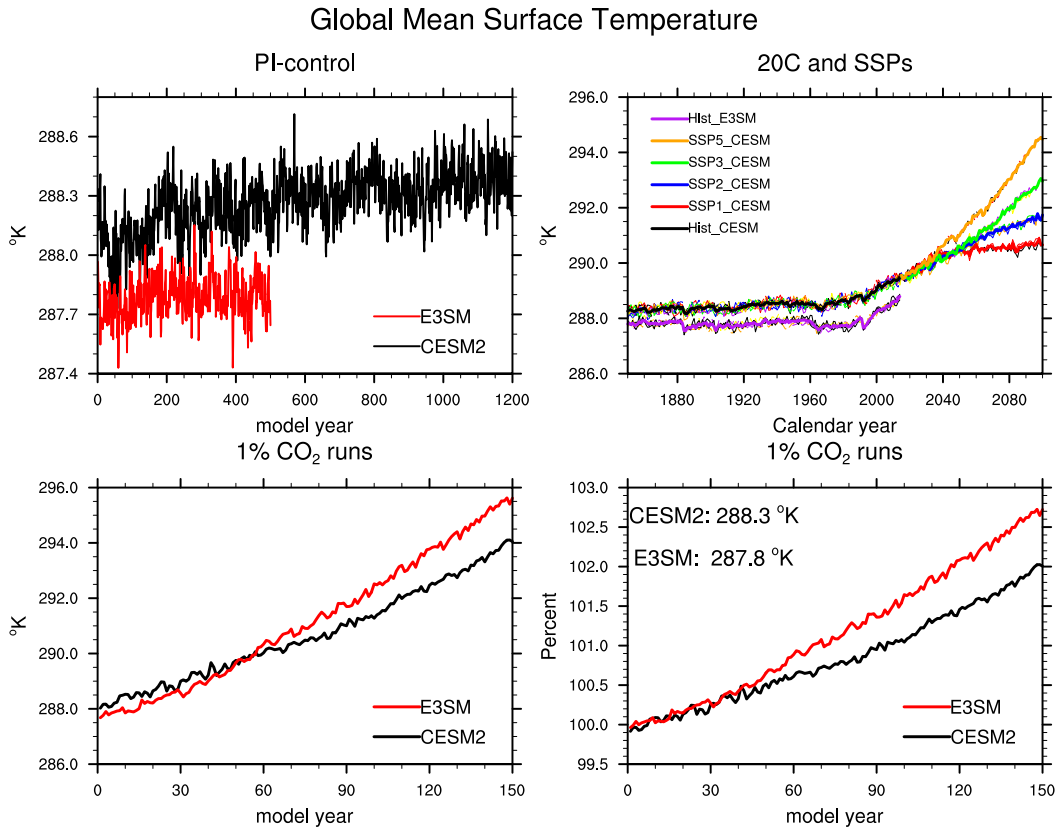

FIG. 3. The global mean surface temperature changes in the (top left) preindustrial control runs, (top right) twentieth-century and SSP runs, and (bottom left) the 1% CO_2 runs and (bottom right) the percentage changes relative to the control run mean in 1% CO_2 runs.

NADW) and slightly weaker bottom cell (related to the AABW formation) in CESM2 than in E3SM1. As AMOC weakens due to the elevated greenhouse gas concentration, the upper cell weakens with a strengthening of the bottom cell for CESM2. However, the changes of the Atlantic meridional streamfunction are different in E3SM1, where the upper portion of the bottom cell strengthens slightly but the lower portion of it weakens, indicating that as CO_2 concentration increases the lighter portion of AABW formation enhances with a weakening of the densest AABW formation in E3SM1. These different changes of AMOC and AABW are associated with different responses of the surface climate to the rising of the atmospheric CO_2 concentration, which will be addressed further later (section 3d).

b. *Global mean and regional surface temperature changes*

The global mean surface air temperature from the preindustrial control runs, twentieth-century historical runs, SSP runs, and 1% CO_2 runs is shown in Fig. 3 (the thick lines are the ensemble mean and thin lines are the individual members). The global mean temperature in the control runs is 288.3 K for CESM2 and 287.8 K for E3SM1, so the preindustrial mean climate in E3SM1 is about 0.5 K cooler than that in CESM2. Over the 1200 years, the surface climate has a small warming trend (0.025 K century^{-1}) in CESM2; however, for E3SM1 this trend is only 0.013 K century^{-1} in the 500-yr-long control run due to choices made in tuning E3SM1 (Golaz et al. 2019). These small trends are related to the top-of-atmosphere radiation imbalance and the heat exchange between deeper ocean and the surface.

In the historical simulations, the time evolution of the global mean temperature varies in a very similar way in CESM2 and E3SM1. The overall rise of the global mean temperature is a few tens of a degree higher in CESM2 relative to E3SM1 (1.14 vs 0.88 K averaged over 2010–14 across all ensemble members). In CESM2, the increase in global mean temperature by the end of the twenty-first century is 2.43 K for SSP1–2.6, 3.35 K for SSP2–4.5, 4.49 K for SSP3–7.0, and 6.02 K for SSP5–8.5 averaged over 2091–2100. To compare more objectively between

these two models, we investigate the global mean temperature changes in the 1% CO_2 simulations where the only forcing varied with time is the CO_2 concentration in the atmosphere. As shown in bottom panels of Fig. 3, the increase in global mean temperature is higher (both absolute values and percentagewise) in E3SM1 than in CESM2 averaged over the times of CO_2 doubling and quadrupling (2.97 vs 2.05 K for doubling CO_2 and 7.24 vs 5.24 K for quadrupling CO_2). As indicated by previous studies, the equilibrium climate sensitivity (ECS; based on the Gregory method; Gregory et al. 2004) in both CESM2 and E3SM1 is 5.3 K (Gettelman et al. 2019; Golaz et al. 2019). The different rate of warming in the 1% CO_2 simulations in these two models suggests that the transient response of the climate system could be significantly different from equilibrium response, and that the ECS is not a good indicator of transient climate sensitivity (defined as the global mean surface temperature change at time of CO_2 doubling in the 1% CO_2 run, an average between model years 61 and 80). Since the external forcing is the same for both models, these differences must be related to the internal climate processes and how these processes would respond to the changes in greenhouse gas forcing.

The regional temperature patterns in both control simulations are very similar to each other (top two panels in Fig. 4); however, the Northern Hemisphere is overall warmer in CESM2 than in E3SM1, especially in the subpolar North Atlantic region (top panel in Fig. 5, which is the difference between the left and right panels in Fig. 4). This pattern of surface temperature difference between these two models (top panel in Fig. 5) is very similar to the surface temperature change pattern with a strengthening of the AMOC (e.g., Stouffer et al. 2006; Hu et al. 2010, 2013, 2015). With a stronger AMOC, more heat is transported into the North Atlantic region, leading to a warmer North Atlantic and the surrounding regions, even the whole Northern Hemisphere (Rugenstein et al. 2013). This result suggests that the surface air temperature difference between these two models is in part related to a stronger AMOC in CESM2 than that in E3SM1.

In response to the rising CO_2 concentration, the surface climate warms up almost everywhere in both models, except in the subpolar North Atlantic region in CESM2 where it shows a cooler temperature relative to the preindustrial climate (middle-left and bottom-left panels in Fig. 4). This cooler temperature has been seen in previous simulations from models participating CMIP3 and CMIP5 (Meehl et al. 2007; Collins et al. 2013) and has been demonstrated to be associated with the weakening of the AMOC (e.g., Drijfhout 2010; Hu et al. 2011, 2013; Winton et al. 2013). Polar amplified warming is significantly bigger in E3SM1 than in CESM2, especially at the time of CO_2 quadrupling. Overall, the warming in CESM2 in response to the rising CO_2 concentration is less than that in E3SM1 almost everywhere, particularly in the Northern Hemisphere mid- to high latitudes (Fig. 5, middle and bottom panels). If the global mean difference is subtracted from the middle and bottom panels of Fig. 5, the reduced warming in CESM2 in comparison to E3SM1 is much larger in the Northern Hemisphere than that in the Southern Hemisphere. In other words, this reduced warming in CESM2 is much less than the global mean reduced warming in the Northern Hemisphere and a slightly above that in the Southern Hemisphere, a pattern similar to that induced by a weakening of AMOC (e.g., Stouffer et al. 2006; Hu et al. 2011). Therefore, this overall reduced warming in response to the same rate of CO_2 increase in CESM2 relative to E3SM1 is primarily induced by the much significant decline of the AMOC to rising CO_2 in CESM2 than in E3SM1.

c. *Possible causes for a weaker AMOC in E3SM1 in comparison to that in CESM2*

It is important to understand why the AMOC is significantly weaker in E3SM1 than in CESM2. Figure 6 shows the winter mixed layer (MLD) depth difference between CESM2 and E3SM1 (March MLD for Northern Hemisphere and September MLD for Southern Hemisphere). In general, the MLD is deeper in CESM2 than in E3SM1 almost everywhere, especially in the subpolar North Atlantic. A deeper winter mixed layer is an indicator of a stronger water mass exchange between the surface ocean and the subsurface/deep ocean or an overall weaker oceanic stratification. The winter MLD mean state in these two models (Fig. S1 in the online supplemental material) shows that there is no deep convection in the Labrador and Irminger Seas in E3SM1 (with mixed layer depth less than 300 m), where all its deep convection occurs in the Greenland–Iceland–Norwegian Seas (GIN Seas; with mixed layer depth over 500 m). This pattern of deep convection does not agree with observations (e.g., Smethie et al. 2000; Tanhua et al. 2005). On the other hand, the winter mixed layer is over 1000 m deep in the Labrador and Irminger Seas and over 500 m in the GIN Seas, suggesting that deep convection in CESM2 occurs in both GIN Seas and the Labrador and Irminger Seas, agreeing with the observations (e.g., Smethie et al. 2000; Tanhua et al. 2005). Lack of deep convection in the Labrador and Irminger Seas in E3SM1 is consistent with its weak AMOC, which was also noted in Golaz et al. (2019).

A comparison of the sea surface temperature (SST) and salinity (SSS) between these two models in the preindustrial control runs suggests that in the subpolar

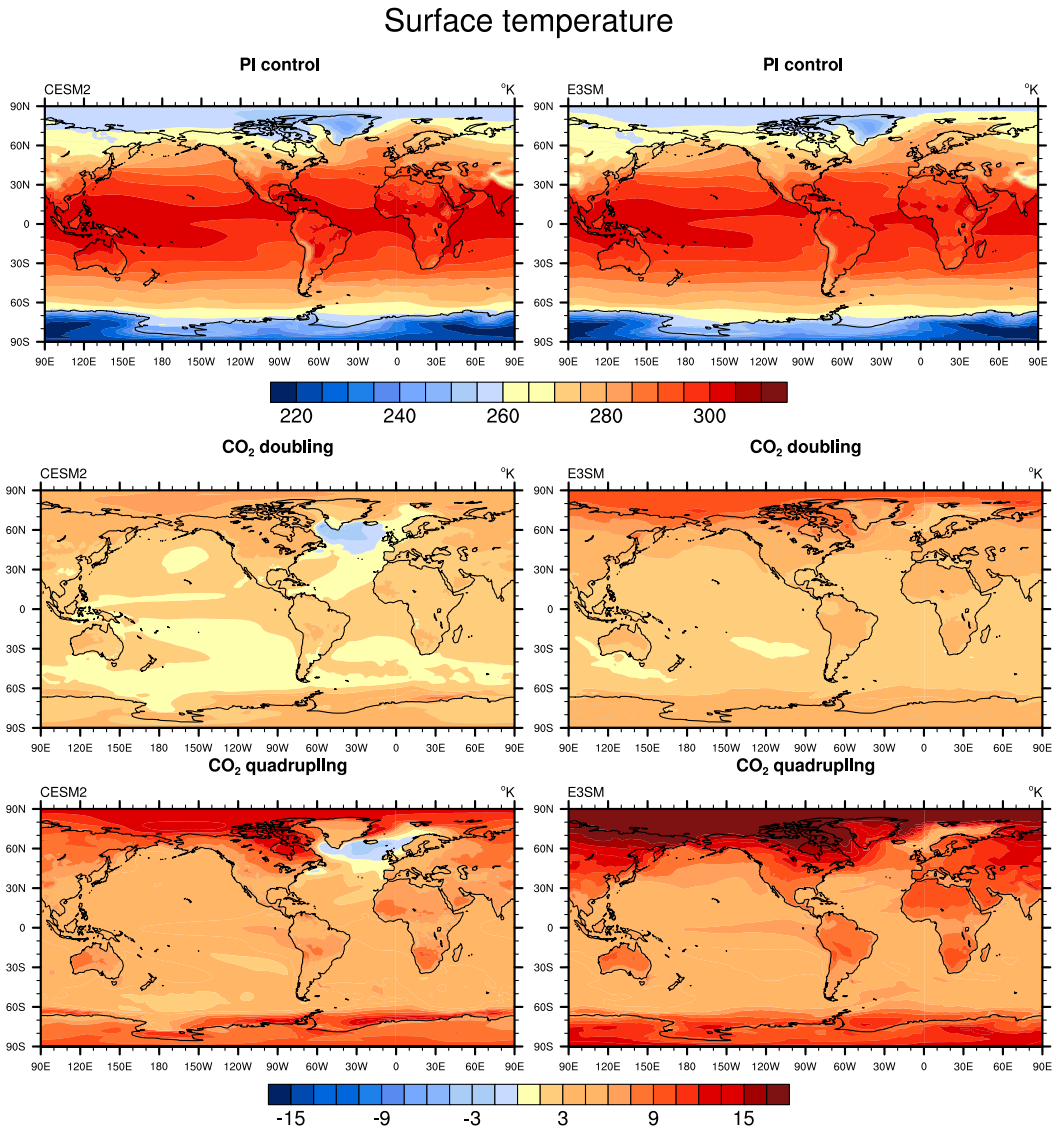

FIG. 4. (top) Mean surface temperature in control run and the mean temperature changes in the 1% CO_2 runs at times of CO_2 (middle) doubling and (bottom) quadrupling. The contour interval for the control runs is 5 K and for the temperature anomaly is 1.5 K.

North Atlantic, the surface water is warmer and more saline in CESM2 than in E3SM1 (top two panels in Fig. 7 and Fig. S2), which is consistent with an excessive sea ice bias in the Labrador and Irminger Seas in E3SM1 (Golaz et al. 2019) that is not evident in CESM2. The melt of this excess ice during boreal summer in E3SM1 results in a cold bias of up to 5°C in E3SM1 relative to CESM2 and an SSS bias up to 3–5 psu (practical salinity units) lower in E3SM1 than in CESM2. It is possible that this fresher and cooler water in E3SM1 prevents the deep convection in the subpolar North Atlantic, reducing the strength of AMOC in E3SM1. This fresher and cooler water is further amplified due to the feedback of the weaker AMOC in E3SM1, which transports significantly less heat and salt (from the subtropical region) into the subpolar region. The surface freshwater input in this region is, in fact, much larger (up to 1 mm day^{-1}) in E3SM1 than in CESM2, which is again consistent with excess sea ice formation and melting and larger precipitation minus evaporation in the North Atlantic in E3SM1. However, in the GIN Seas, the freshwater input is much less (up to 3 mm day^{-1}) in E3SM1 than in CESM2, which is responsible for a stronger deep convection there in E3SM1.

To check whether this biased ocean stratification would affect the zonal mean water mass property, we

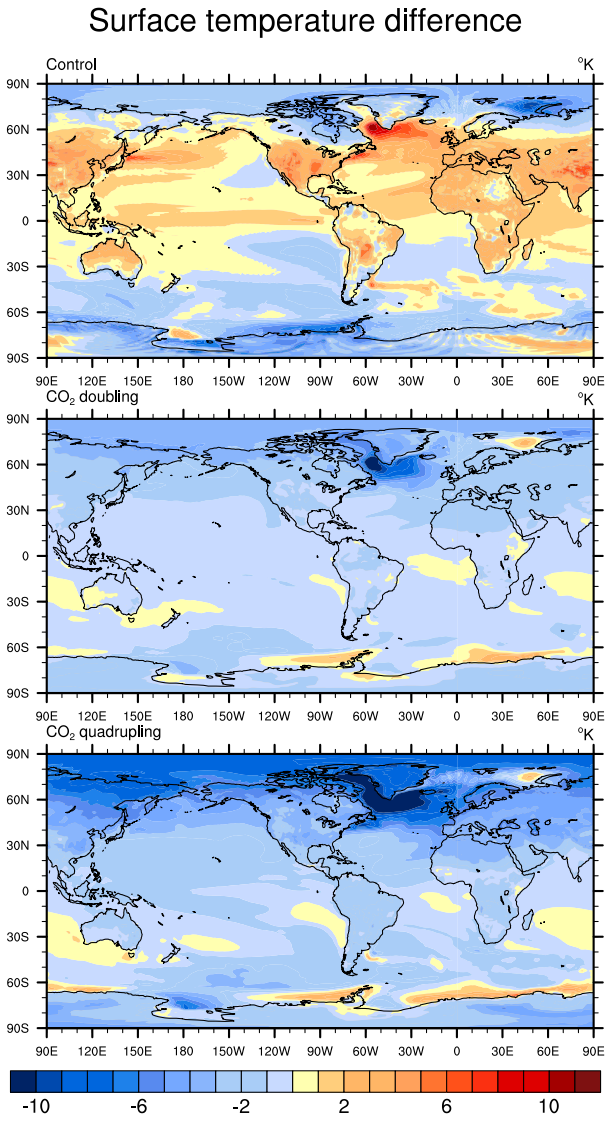

FIG. 5. Surface temperature difference between CESM2 and E3SM1 in (top) the control run, and in the 1% CO_2 run at times of CO_2 (middle) doubling and (bottom) quadrupling. The contour interval is 1 K.

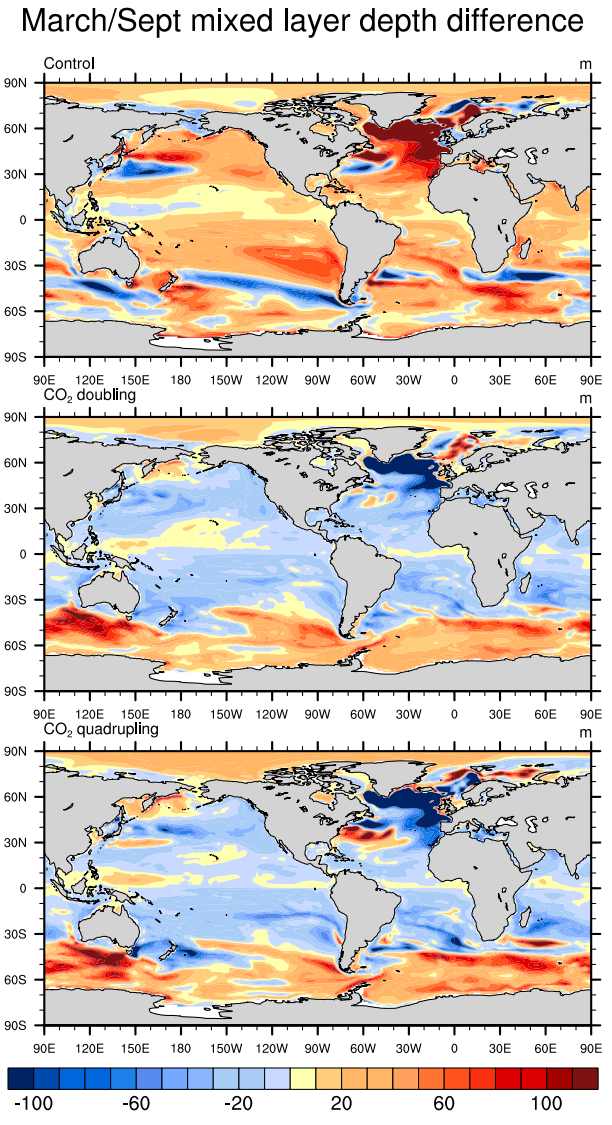

FIG. 6. Winter mixed layer depth difference between CESM2 and E3SM1 in (top) the control run (CESM2 minus E3SM1) and in the 1% CO_2 run at times of CO_2 (middle) doubling and (bottom) quadrupling. The contour interval is 10 m.

analyze the zonal mean salinity in the Atlantic (Fig. 8). It shows a clear signature of the NADW formation and the high-salinity water in the middepth ocean in association to the NADW pathway and the lower-salinity Antarctic Intermediate Water subducted around 55°S to a depth about 1000 m and flowing northward in CESM2 (Fig. 8), a feature that agrees very well with observations (Reid 1994). In E3SM1, there is no clear signature of the low-salinity Antarctic Intermediate Water and the signature of the NADW is also not as clear as in CESM2. The upper 200 m ocean north of 40°N is much fresher in E3SM1 than CESM2, consistent with the lack of deep convection in Labrador and Irminger Seas in E3SM1. Because the lower boundary of AMOC is much shallower in E3SM1, the penetration of the high-salinity water (salinity above 35 psu) is only to a depth of about 1000 m, but to about 2000 m in CESM2. These features suggest that not only is the AMOC in E3SM1 weaker than in CESM2, but also the vertical structure of the AMOC is biased in comparison to observations. These biases of vertical salinity pattern in E3SM1 might be a result of the overall weaker AMOC and feedbacks between a weaker AMOC and the surface climate.

In summary, it is the fresher surface water in association to a higher surface freshwater input in the subpolar North Atlantic, which leads to a less dense surface water

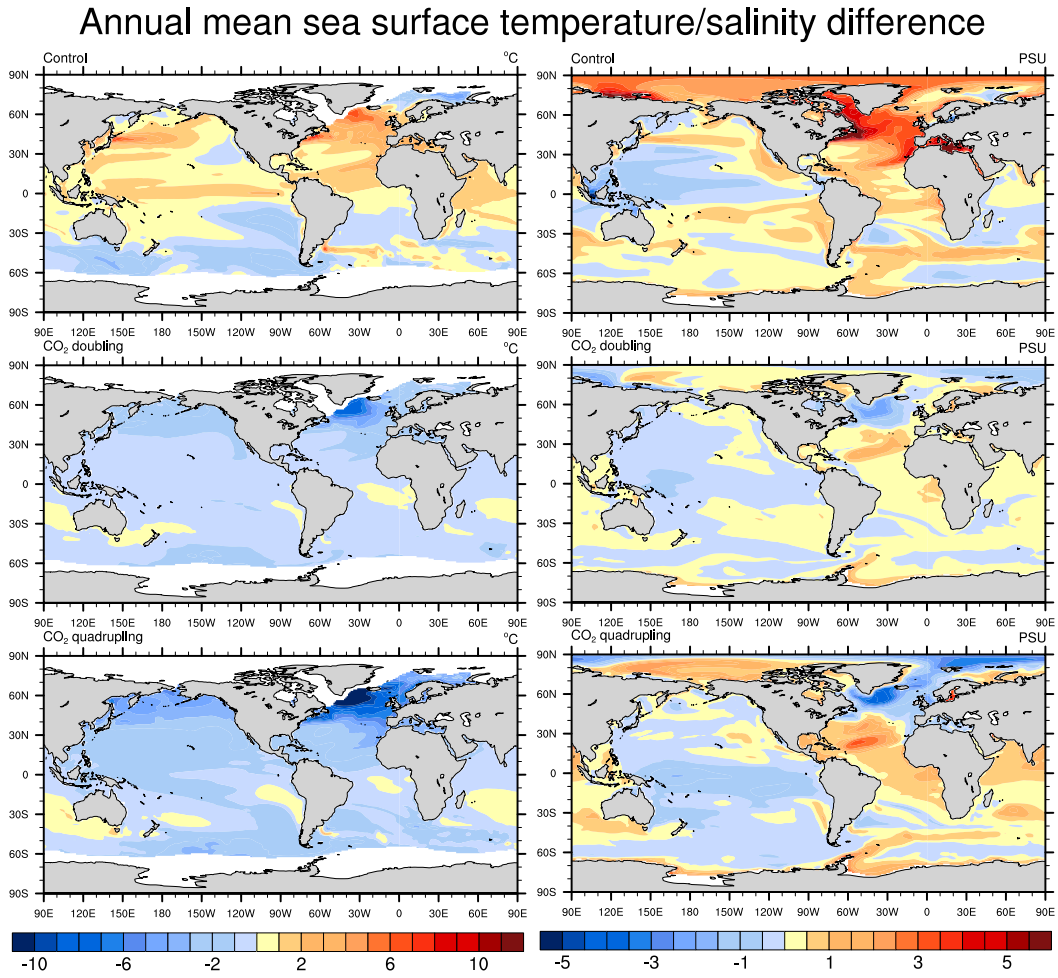

FIG. 7. Annual mean sea surface (left) temperature (SST) and (right) salinity (SSS) difference between CESM2 and E3SM1 in (top) the control run, and in the 1% CO_2 run at times of CO_2 (middle) doubling and (bottom) quadrupling. The contour interval is 1 K for the left column and 0.5 psu for the right column.

in this region and prevents the occurrence of deep convection in this region in E3SM1. Although the deep convection is slightly stronger in GIN Seas in E3SM1, this is still not enough to compensate for the lack of the deep water formation in the Labrador and Irminger Seas, producing a weaker AMOC in E3SM1 than in CESM2. This weaker AMOC also feeds back to the upper-ocean property. By transporting less subtropical saline water to the subpolar North Atlantic, AMOC also indirectly contributes to the low salinity bias in this region in E3SM1.

While it is likely that the fresher surface water associated with a higher surface freshwater input in the subpolar North Atlantic contributes to the reduced AMOC in E3SM1, sensitivity tests conducted during development of E3SM version 2 suggest that this does not completely explain the weak AMOC in E3SM. In these test experiments (not shown), the surface freshwater input is dramatically improved and the SSS biases seen in Fig. 7 are greatly reduced, yet the AMOC only improves by ~1 Sv. Oddly, despite the improvement of upper-ocean salinity, the deep convection in the Labrador and Irminger Seas remains weak, suggesting it is still possible that the lack of deep convection in these areas contributes to the weak AMOC in E3SM1. It is also possible that a lack of overflow parameterization (e.g., Yeager et al. 2012) in E3SM1, differences in abyssal mixing parameterizations, or formulations of the mesoscale eddy parameterizations (e.g., the Gent and McWilliams parameterization; Gent and McWilliams 1990) could further contribute to the weak AMOC in E3SM1. Thus, understanding the weak AMOC in E3SM remains an active and critical area of research, but beyond the scope of this study.

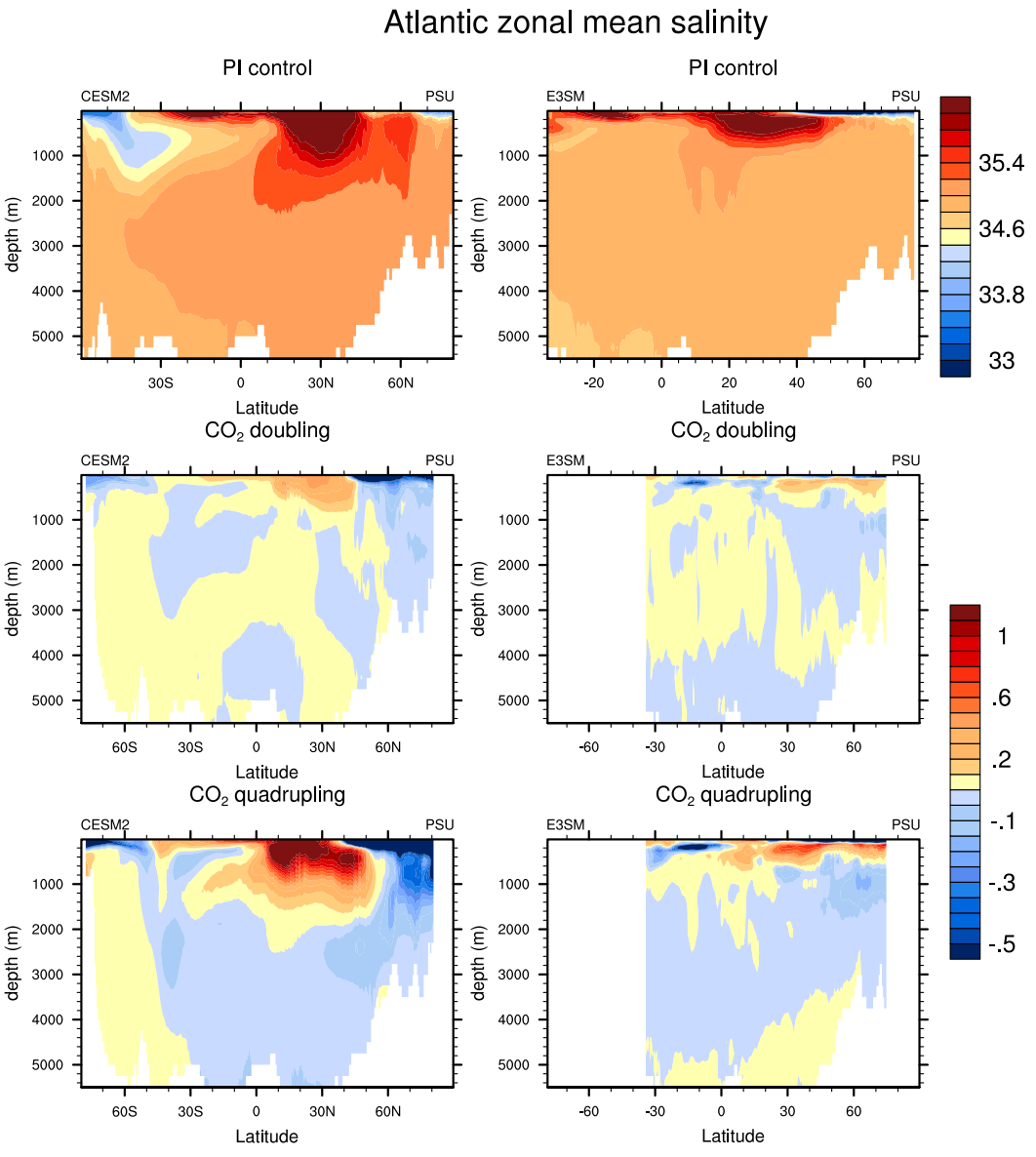

FIG. 8. (top) Atlantic zonal mean salinity in control runs, and the zonal mean salinity anomaly in the 1% CO_2 runs at times of CO_2 (middle) doubling and (bottom) quadrupling. The contour interval is 0.2 psu for the control runs, and 0.1 psu for positive anomalies and 0.05 psu for negative anomalies for the 1% CO_2 runs.

d. Role of AMOC in response of surface climate to elevated greenhouse gas concentrations

As we have discussed earlier, the ECS in both models is the same, but the transient climate response is much larger in E3SM1 than in CESM2. Although there are a number of differences in model formulation between these two models, the most obvious difference in their preindustrial control simulation is the strength of the AMOC. Therefore, the differences in transient climate response to the rising of atmospheric CO_2 concentration could at least be partially due to the AMOC, which we will illustrate in more detail here.

A weaker and shallower AMOC, in general, will lead to a stronger upper-ocean stratification, at least in the Atlantic basin. A stronger upper-ocean stratification will reduce the formation of deep water masses. As the atmospheric CO_2 concentration increases, the warming of the upper ocean will further strengthen the oceanic stratification, and make the heat exchange and formation of deep water masses be even less sufficient. If these basic physical processes are at work, we would expect that the subsurface warming in the 1% CO_2 runs will be less in E3SM1 than in CESM2. The global zonal mean temperature in the control runs shows that the deeper

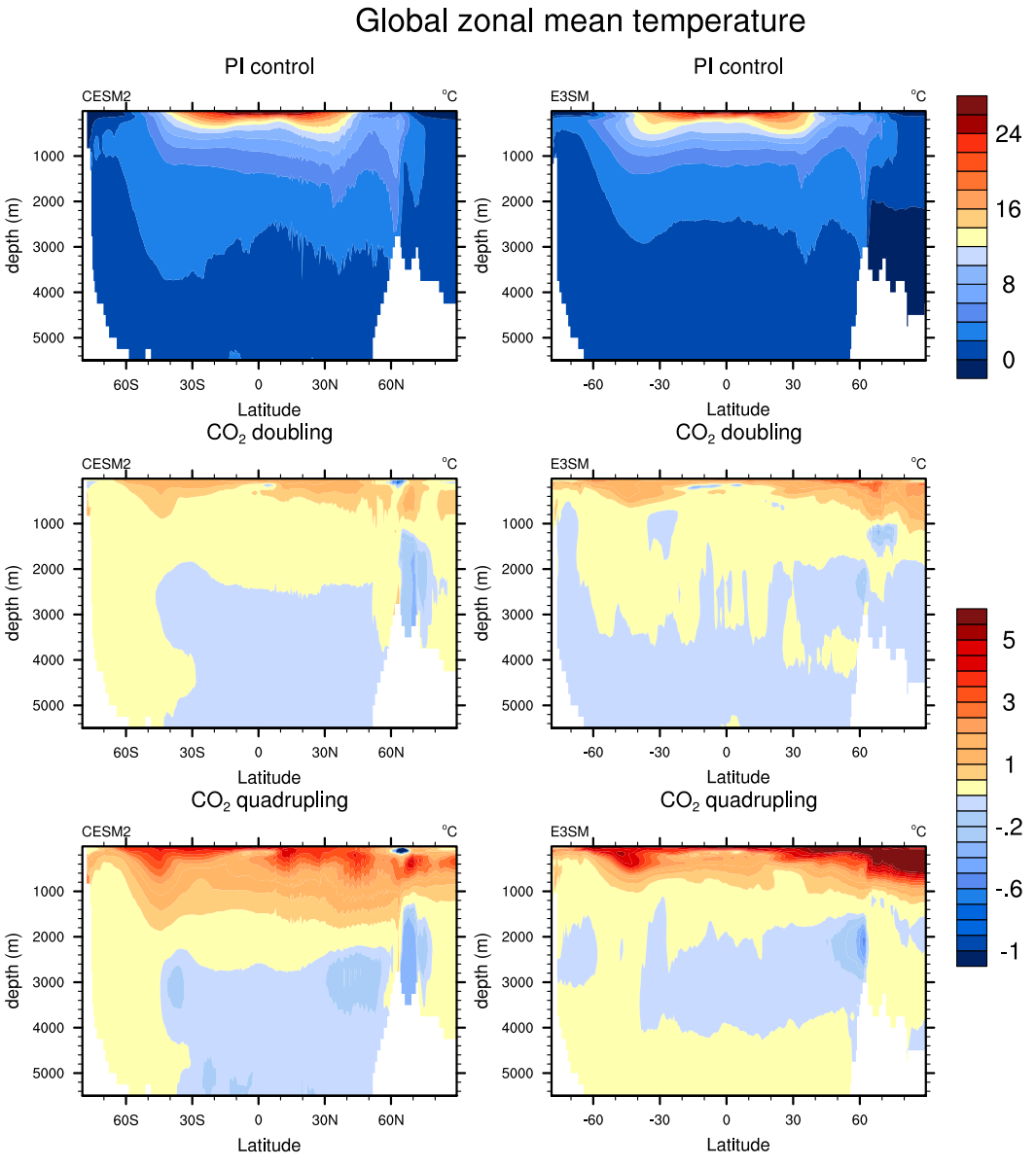

FIG. 9. (top) Global zonal mean temperature in control runs, and the zonal mean temperature anomaly in the 1% CO_2 runs at times of CO_2 (middle) doubling and (bottom) quadrupling. The contour interval is 2°C for the control runs, and 0.5°C for positive anomalies and 0.1°C for negative anomalies for the 1% CO_2 runs.

ocean in E3SM1 is colder than that in CESM2 (Fig. 9). In the Atlantic, this temperature difference between these two models is more than 1 K for waters deeper than 500-m depth (not shown). In the 1% CO_2 simulations, the comparison of the oceanic warming between these two models shows that the upper-ocean warming is slightly higher in E3SM1 than in CESM2 at time of CO_2 doubling, but much higher at time of CO_2 quadrupling (bottom four panels in Fig. 9). Moreover, the warming for the water between roughly 500- and 2000-m depth is higher in CESM2 than in E3SM1, especially at time of CO_2 quadrupling. This pattern of the ocean temperature change is even more obvious in the Atlantic zonal mean temperature change (figure not shown), suggesting that the AMOC may indeed play a role in determining the transient climate response to an elevated atmospheric CO_2 concentration.

In response to the rising atmospheric CO_2 concentration, the surface warming is less in CESM2 than in E3SM1 almost everywhere, and the largest discrepancy occurs in the subpolar North Atlantic region with a temperature difference up to 10 K (bottom four panels

in Fig. 4 and bottom two panels in Fig. 5). The pattern of the temperature change difference between these two models shows much less warming in the Northern Hemisphere than in Southern Hemisphere in CESM2, a pattern resembling the surface climate response to a weakening of AMOC. As we have shown earlier, although AMOC is always stronger in CESM2 than E3SM1, AMOC weakens more in CESM2 than in E3SM1 both in absolute value and the percentage. A large decline in AMOC strength will reduce the greenhouse gas–induced warming in the subpolar North Atlantic and the surrounding regions, even the entire Northern Hemisphere (Hu et al 2015). The similarity between the temperature difference of these two models in 1% CO_2 runs and the surface temperature changes in response to a AMOC decline suggests that the difference in transient climate response to the greenhouse gas forcing between these two models is caused by the different response of AMOC in these two models (and the different ocean stratification associated with the different AMOC mean state in the preindustrial control run).

To further demonstrate the effect of AMOC on the transient climate response to greenhouse gas forcing, we will examine the changes of mixed layer depth. As we have indicated earlier, the winter mixed layer is in general deeper in CESM2 than in E3SM1 in the preindustrial control runs (Fig. 6). In response to the rising CO_2 concentration, winter mixed layer depth reduces almost globally in both models with mixed layer deepening only in portions of the Southern Ocean; the latter is associated with a strengthening of the AABW formation as shown in the Atlantic meridional streamfunction (Fig. 2), which is induced by a strengthening of the Southern Ocean westerlies (Hu and Bates 2018). The most significant shoaling of the mixed layer is in the Labrador and Irminger Seas in CESM2, with a maximum reduction over 1400 m in March at the times of CO_2 doubling and quadrupling, indicating a nearly collapsed deep convection in these seas caused by the quick surface warming and freshening (bottom panels in Figs. 8 and 9, and Fig. S1). At the same time, the mixed layer deepens by a couple of hundred meters in GIN Seas when CO_2 concentration doubles, suggesting a strengthening of the deep convection there, which agrees well with previous studies (e.g., Hu et al. 2004). However, at the time of CO_2 quadrupling, the mixed layer becomes shallow in GIN Seas. These results show that the initial response of the mixed depth (strength of the deep convection) is to shoal in the Labrador and Irminger Seas with a deepening in GIN Seas due to the warming in the former region (Gregory et al. 2005) and the more saline upper ocean due to reduced sea ice export from the Arctic and increased inflow of the more saline North Atlantic water for the latter (Hu et al. 2004). Later, the shoaling of mixed layer in GIN Seas is caused by the further surface warming in GIN Seas and increase of the exported melt sea ice water from the Arctic in association to the greenhouse gas forcing.

Because there is no deep convection in the Labrador and Irminger Seas in E3SM1, the weakening of deep convection occurs only in GIN Seas in response to rising CO_2 concentration and this reduction ranges from ~300 to 350 m, about 56% to 66% of the control run depth from CO_2 doubling to CO_2 quadrupling. This shoaling of the mixed layer is nearly basin wide in GIN Seas at time of CO_2 quadrupling.

In comparison to the winter mixed layer depth changes between these two models (lower two panels in Fig. 6), the shoaling of the mixed layer is much larger in most parts of the ocean in CESM2 than that in E3SM1. The winter mixed layer depth in CESM2 changes from about 20–60 m deeper than that in E3SM1 in most tropical to subpolar oceans to about similar depth in some regions (mostly subtropical regions) or only about 20 m deeper. In the southern oceans, the mixed layer is up to 100 m deeper in CESM2 than in E3SM1 in association to the much stronger AABW formation in CESM2 than in E3SM1. In the subpolar North Atlantic, with a significantly larger shoaling of the mixed layer in the 1% CO_2 run than in the control run, the winter mixed layer is still deeper in CESM2 than in E3SM1 in both Labrador and Irminger Seas, and the GIN Seas. This is not only related to the overall less surface warming over this region in CESM2 than in E3SM1, but also related to the overall more saline surface ocean in CESM2 than in E3SM1 in this region (Fig. S2) despite the larger freshening in CESM2. Both of the temperature and salinity changes contribute to a denser surface water in CESM2 than in E3SM1 in the subpolar North Atlantic and an overall stronger AMOC in CESM2 throughout the entire course of the 1% CO_2 runs than that in E3SM1. Therefore, it further demonstrates that the preindustrial mean state of the AMOC (or the ocean stratification) can affect the response of the climate to the rising atmospheric CO_2 concentration, at least in these 1% CO_2 runs.

In summary, these changes in winter mixed layer depth imply that the changes in AMOC may have contributed to the global mixed layer depth variations. As AMOC weakens, the deep convection reduces, leading to a reduced formation of deep water masses. As a result, the upwelling of subsurface colder water in association to AMOC also reduces, further strengthening the global ocean stratification. Therefore, our results suggest that the difference in AMOC mean state and its transient response to the greenhouse gas changes can

significantly affect the transient response of the climate system to the greenhouse gas forcing, agreeing with some of the previous studies (Winton et al. 2013; Kostov et al. 2014; Stolpe et al. 2018).

4. Conclusions

In this work, we have analyzed simulations from two CMIP6 models, CESM2 and E3SM1, focusing on the AMOC and the transient climate response. Our analysis shows that the preindustrial mean AMOC in E3SM1 is about 40% weaker than that in CESM2, and the mean AMOC strength in CESM2 agrees with observations very well. The weaker AMOC in E3SM1 is likely due to a number of factors, including the absence of deep convection (NADW formation) in the Labrador and Irminger Seas. In response to the rising greenhouse gas forcing, warming of the surface climate is faster in E3SM1 than in CESM2 due to a much stronger ocean stratification. This stronger upper-ocean stratification in E3SM1 can be attributed partially to a weaker AMOC, which generates a weaker sinking of the upper-ocean water and a weaker upwelling of deep water. As the climate warms, the stronger stratification in E3SM1 further increases due to a faster surface warming than the warming in subsurface ocean. This results in a much faster warming in the upper ocean and less warming in the subsurface ocean in E3SM1 than in CESM2, which further demonstrates that the AMOC mean state and its transient response to greenhouse gas forcing can modulate the ocean stratification, and further affects the model transient climate response.

In this work, although we have compared the mean strength of the simulated AMOC with observations, we did not compare the detailed structure of the AMOC (including the Gulf Stream) with the observations since this is not the focus of this study. As indicated recently by Seidov et al. (2019), different ocean horizontal resolutions can produce significantly different structure of the AMOC system in observations. A high resolution will produce a much better AMOC system than the one by lower resolution in observations. For both CESM and E3SM, previous studies also indicate that the simulated Gulf Stream is much closer to the observed one in the 1/10° horizontal resolution version of the models than that in the standard 1° version (Bryan et al. 2010; Small et al. 2014; Caldwell et al. 2019). Nevertheless, any detailed comparisons between model simulations and observations are complicated not only by the dependence of the details of the modeled AMOC including the Gulf Stream system and their biases on resolution, but also by the dependence of the details of the observed climatology on the resolution at which it is compiled (e.g., see Seidov et al. 2019).

Acknowledgments. This research was supported by the Regional and Global Model Analysis (RGMA), a component of the Earth and Environmental System Modeling (EESM) program of the U.S. Department of Energy's Office of Science, as a contribution to the HiLAT-RASM project and CATALYST program. Cheng is supported by National Oceanic and Atmospheric Administration (NOAA) Climate Program Office under Climate Variability and Predictability Program, Grants NA15OAR4320063 and NA16OAR4310169. This research was supported as part of the Energy Exascale Earth System Model (E3SM) project, funded by the U.S. Department of Energy, Office of Science, Office of Biological and Environmental Research. The National Center for Atmospheric Research is sponsored by the National Science Foundation.

REFERENCES

Barker, S., P. Diz, M. J. Vautravers, J. Pike, G. Knorr, I. R. Hall, and W. S. Broecker, 2009: Interhemispheric Atlantic seesaw response during the last deglaciation. *Nature*, **457**, 1097–1102, https://doi.org/10.1038/nature07770.

Broecker, W. S., 1998: Paleocean circulation during the last deglaciation: A bipolar seesaw? *Paleoceanography*, **13**, 119–121, https://doi.org/10.1029/97PA03707.

Bryan, F. O., R. Tomas, J. M. Dennis, D. B. Chelton, N. G. Loeb, and J. L. McClean, 2010: Frontal scale air–sea interaction in high-resolution coupled climate models. *J. Climate*, **23**, 6277–6291, https://doi.org/10.1175/2010JCLI3665.1.

Caldwell, P. M., and Coauthors, 2019: The DOE E3SM coupled model version 1: Description and results at high resolution. *J. Adv. Model. Earth Syst.*, **11**, 4095–4146, https://doi.org/10.1029/2019MS001870.

Cheng, W., J. C. Chiang, and D. Zhang, 2013: Atlantic meridional overturning circulation (AMOC) in CMIP5 models: RCP and historical simulations. *J. Climate*, **26**, 7187–7197, https://doi.org/10.1175/JCLI-D-12-00496.1.

Collins, M., and Coauthors, 2013: Long-term climate change: Projections, commitments and irreversibility. *Climate Change 2013: The Physical Science Basis*, T. F. Stocker et al., Eds., Cambridge University Press, 1029–1136.

Cunningham, S. A., and R. Marsh, 2010: Observing and modeling changes in the Atlantic MOC. *Wiley Interdiscip. Rev.: Climate Change*, **1**, 180–191, https://doi.org/10.1002/WCC.22.

——, and Coauthors, 2007: Temporal variability of the Atlantic meridional overturning circulation at 26.5°N. *Science*, **317**, 935–938, https://doi.org/10.1126/science.1141304.

——, and Coauthors, 2013: Atlantic Meridional Overturning Circulation slowdown cooled the subtropical ocean. *Geophys. Res. Lett.*, **40**, 6202–6207, https://doi.org/10.1002/2013GL058464.

Danabasoglu, G., and Coauthors, 2019: The Community Earth System Model version 2 (CESM2). *J. Adv. Model. Earth Syst.*, **12**, e2019MS001916, https://doi.org/10.1029/2019MS001916.

Drijfhout, S. S., 2010: The atmospheric response to a thermohaline circulation collapse: Scaling relations for the Hadley circulation and the response in a coupled climate model. *J. Climate*, **23**, 757–774, https://doi.org/10.1175/2009JCLI3159.1.

Eyring, V., S. Bony, G. A. Meehl, C. A. Senior, B. Stevens, R. J. Stouffer, and K. E. Taylor, 2016: Overview of the Coupled

Model Intercomparison Project Phase 6 (CMIP6) experimental design and organization. *Geosci. Model Dev.*, **9**, 1937–1958, https://doi.org/10.5194/gmd-9-1937-2016.

Gent, P. R., and J. C. McWilliams, 1990: Isopycnal mixing in ocean circulation models. *J. Phys. Oceanogr.*, **20**, 150–155, https://doi.org/10.1175/1520-0485(1990)020<0150:IMIOCM>2.0.CO;2.

Gettelman, A., and Coauthors, 2019: High climate sensitivity in the Community Earth System Model version 2 (CESM2). *Geophys. Res. Lett.*, **46**, 8329–8337, https://doi.org/10.1029/2019GL083978.

Golaz, J. C., and Coauthors, 2019: The DOE E3SM1 coupled model version 1: Overview and evaluation at standard resolution. *J. Adv. Model. Earth Syst.*, **11**, 2089–2129, https://doi.org/10.1029/2018MS001603.

Gregory, J. M., and Coauthors, 2004: A new method for diagnosing radiative forcing and climate sensitivity. *Geophys. Res. Lett.*, **31**, L03205, https://doi.org/10.1029/2003GL018747.

——, and Coauthors, 2005: A model intercomparison of changes in the Atlantic thermohaline circulation in response to increasing atmospheric CO_2 concentration. *Geophys. Res. Lett.*, **32**, L12703, https://doi.org/10.1029/2005GL023209.

Hu, A., and S. C. Bates, 2018: Internal climate variability and projected future regional steric and dynamic sea level rise. *Nat. Commun.*, **9**, 1068, https://doi.org/10.1038/s41467-018-03474-8.

——, G. A. Meehl, W. M. Washington, and A. Dai, 2004: Response of the Atlantic thermohaline circulation to increased atmospheric CO_2 in a coupled model. *J. Climate*, **17**, 4267–4279, https://doi.org/10.1175/JCLI3208.1.

——, B. L. Otto-Bliesner, G. A. Meehl, W. Han, C. Morrill, E. C. Brady, and B. Briegleb, 2008: Response of thermohaline circulation to freshwater forcing under present day and LGM conditions. *J. Climate*, **21**, 2239–2258, https://doi.org/10.1175/2007JCLI1985.1.

——, and Coauthors, 2010: Influence of Bering Strait flow and North Atlantic circulation on glacial sea-level changes. *Nat. Geosci.*, **3**, 118–121, https://doi.org/10.1038/ngeo729.

——, G. A. Meehl, W. Han, and J. Yin, 2011: Effect of the potential melting of the Greenland Ice Sheet on the meridional overturning circulation and global climate in the future. *Deep-Sea Res. II*, **58**, 1914–1926, accessed October 2019, https://doi.org/10.1016/j.dsr2.2010.10.069.

——, and Coauthors, 2012: Role of the Bering Strait on the hysteresis of the ocean conveyor belt circulation and glacial climate stability. *Proc. Natl. Acad. Sci. USA*, **109**, 6417–6422, https://doi.org/10.1073/pnas.1116014109.

——, G. A. Meehl, W. Han, J. Yin, B. Wu, and M. Kimoto, 2013: Influence of continental ice retreat on future global climate. *J. Climate*, **26**, 3087–3111, https://doi.org/10.1175/JCLI-D-12-00102.1.

——, ——, ——, B. Otto-Bliesner, A. Abe-Ouchi, and N. Rosenbloom, 2015: Effects of the Bering Strait closure on AMOC and global climate under different background climates. *Prog. Oceanogr.*, **132**, 174–196, https://doi.org/10.1016/j.pocean.2014.02.004.

Hurrell, J. W., and Coauthors, 2013: The Community Earth System Model: A framework for collaborative research. *Bull. Amer. Meteor. Soc.*, **94**, 1339–1360, https://doi.org/10.1175/BAMS-D-12-00121.1.

Johns, W. E., and Coauthors, 2011: Continuous, array-based estimates of Atlantic Ocean heat transport at 26.5°N. *J. Climate*, **24**, 2429–2449, https://doi.org/10.1175/2010JCLI3997.1.

Kostov, Y., K. C. Armour, and J. Marshall, 2014: Impact of the Atlantic meridional overturning circulation on ocean heat storage and transient climate change. *Geophys. Res. Lett.*, **41**, 2108–2116, https://doi.org/10.1002/2013GL058998.

Lin, Y.-J., Y.-T. Hwang, P. Ceppi, and J. M. Gregory, 2019: Uncertainty in the evolution of climate feedback traced to the strength of the Atlantic meridional overturning circulation. *Geophys. Res. Lett.*, **46**, 12 331–12 339, https://doi.org/10.1029/2019GL083084.

Meehl, G. A., and Coauthors, 2007: Global climate projections. *Climate Change 2007: The Physical Science Basis*, S. Solomon et al., Eds., Cambridge University Press, 747–845.

Petersen, M. R., and Coauthors, 2019: An evaluation of the ocean and sea ice climate of E3SM using MPAS and interannual CORE-II forcing. *J. Adv. Model. Earth Syst.*, **11**, 1438–1458, https://doi.org/10.1029/2018MS001373.

Rahmstorf, S., 1996: On the freshwater forcing and transport of the Atlantic thermohaline circulation. *Climate Dyn.*, **12**, 799–811, https://doi.org/10.1007/s003820050144.

Reid, J. L., 1994: On the total geostrophic circulation of the North Atlantic Ocean: Flow patterns, tracers and transports. *Prog. Oceanogr.*, **33**, 1–92, https://doi.org/10.1016/0079-6611(94)90014-0.

Rugenstein, M. A. A., M. Winton, R. J. Stouffer, S. M. Griffies, and R. Hallberg, 2013: Northern high-latitude heat budget decomposition and transient warming. *J. Climate*, **26**, 609–621, https://doi.org/10.1175/JCLI-D-11-00695.1.

Seidov, D., A. Mishonov, J. Reagan, and R. Parsons, 2019: Eddy-resolving in situ ocean climatologies of temperature and salinity in the northwest Atlantic Ocean. *J. Geophys. Res. Oceans*, **124**, 41–58, https://doi.org/10.1029/2018JC014548.

Small, R. J., and Coauthors, 2014: A new synoptic scale resolving global climate simulation using the Community Earth System Model. *J. Adv. Model. Earth Syst.*, **6**, 1065–1094, https://doi.org/10.1002/2014MS000363.

Smeed, D., B. Moat, D. Rayner, W. E. Johns, M. O. Baringer, D. Volkov, and E. Frajka-Williams, 2019: Atlantic meridional overturning circulation observed by the RAPID-MOCHA-WBTS (RAPID-Meridional Overturning Circulation and Heatflux Array–Western Boundary Time Series) array at 26°N from 2004 to 2018. British Oceanographic Data Centre, National Oceanography Centre, NERC, accessed October 2019, https://doi.org/10.5285/8cd7e7bb-9a20-05d8-e053-6c86abc012c2.

Smethie, W. M., R. A. Fine, A. Putzka, and E. P. Jones, 2000: Tracing the flow of North Atlantic Deep Water using chlorofluorocarbons. *J. Geophys. Res.*, **105**, 14 297–14 323, https://doi.org/10.1029/1999JC900274.

Stocker, T. F., and D. G. Wright, 1991a: A zonally averaged ocean model for the thermoshaline circulation. Part II: Interocean circulation in the Pacific–Atlantic basin system. *J. Phys. Oceanogr.*, **21**, 1725–1739, https://doi.org/10.1175/1520-0485(1991)021<1725:AZAOMF>2.0.CO;2.

——, and ——, 1991b: Rapid transitions of the ocean's deep circulation induced by changes in surface water fluxes. *Nature*, **351**, 729–732, https://doi.org/10.1038/351729a0.

——, L. A. Mysak, and D. G. Wright, 1992: A zonally averaged, coupled ocean–atmosphere model for paleoclimate studies. *J. Climate*, **5**, 773–797, https://doi.org/10.1175/1520-0442(1992)005<0773:AZACOA>2.0.CO;2.

Stolpe, M. B., I. Medhaug, J. Sedlacek, and R. Knutti, 2018: Multidecadal variability in global surface temperatures related to the Atlantic meridional overturning circulation. *J. Climate*, **31**, 2889–2906, https://doi.org/10.1175/JCLI-D-17-0444.1.

Stouffer, R. J., and Coauthors, 2006: Investigating the causes of the response of the thermohaline circulation to past and future climate changes. *J. Climate*, **19**, 1365–1387, https://doi.org/10.1175/JCLI3689.1.

Tanhua, T., K. A. Olsson, and E. Jeansson, 2005: Formation of Denmark Strait overflow water and its hydro-chemical composition. *J. Mar. Syst.*, **57**, 264–288, https://doi.org/10.1016/j.jmarsys.2005.05.003.

Weijer, W., and Coauthors, 2019: Stability of the Atlantic Meridional Overturning Circulation: A review and synthesis. *J. Geophys. Res. Oceans*, **124**, 5336–5375, https://doi.org/10.1029/2019JC015083.

——, W. Cheng, O. Garuba, A. Hu and B. T. Nadiga, 2020: CMIP6 models predict significant 21st century decline of the Atlantic Meridional Overturning Circulation. *Geophys. Res. Lett.*, https://doi.org/10.1029/2019GL086075, in press.

Winton, M., S. M. Griffies, B. L. Samuels, J. L. Sarmiento, and T. L. Frölicher, 2013: Connecting changing ocean circulation with changing climate. *J. Climate*, **26**, 2268–2278, https://doi.org/10.1175/JCLI-D-12-00296.1.

Yeager, S., A. Karspeck, G. Danabasoglu, J. Tribbia, and H. Teng, 2012: A decadal prediction case study: Late twentieth-century North Atlantic Ocean heat content. *J. Climate*, **25**, 5173–5189, https://doi.org/10.1175/JCLI-D-11-00595.1.